Regular Article

PHYSICAL CHEMISTRY RESEARCH
Published by the
Iranian Chemical Society
www.physchemres.org
info@physchemres.org

Phys. Chem. Res., Vol. 11, No. 4, 761-770, December 2023
DOI: 10.22036/pcr.2022.338670.2084

Deactivation of Iron Fischer-Tropsch Catalyst in the Presence of Different Promoters: Model Determination and Parameter Estimation Using a Hybrid ANN/GPLE Technique

M. Ghofran Pakdel[a], S.H. Zohdi[a,*] and A.A. Mirzaei[b]

[a]*Department of Chemical Engineering, Faculty of Engineering, University of Sistan and Baluchestan, P. O. Box: 98164-161, Zahedan, Iran*

[b]*Department of Chemistry, Faculty of Sciences, University of Sistan and Baluchestan, P. O. Box: 98135-674, Zahedan, Iran*

(Received 23 April 2022, Accepted 17 November 2022)

In this paper, the deactivation of the iron-based catalyst was assessed in the presence of Zr, Mn, and Cr promoters at two different loadings (5 and 10%). ANN/GPLE hybrid technique was applied for model determination and parameter estimation, as well as calculation of catalyst stability in the following conditions: temperature = 280 °C, H_2/CO = 2, and pressure = 1.8 atm. The results showed that the promoter loading could change the deactivation behavior of the iron catalyst such that the first-order GPLE model well fitted the results at a promoter loading of 5%. For the case of 10% loading, the second-order GPLE model well fitted the results. A decline in the promoter loading on the iron catalysts enhanced the catalyst stability and decreased its deactivation constant (k_d). The promoter loadings of 5% and 10% indicated coking and sintering mechanisms, respectively. Among the different promoters at various loadings, Mn promoter at the loading of 5% could significantly prolong the catalyst lifetime and enhance the stability of the iron catalyst. Zr increased the deactivation constant of Fe catalyst (k_d) more than other promoters. ANN/GPLE technique is a promising method for the catalytic deactivation investigation, model determination, and parameter estimation.

Keywords: Deactivation models, Iron catalyst, Stability, Artificial neural network, GPLE, Promoter

INTRODUCTION

International predictions in 2018 have estimated a 50% increase in the global fuel generation for transportation supply by 2040 [1]. The rising energy consumption and its impact on greenhouse gas emission, shortage of resources, and global warming have increased awareness of renewable sources of energy [2,3]. Among the renewable sources of energy, biomass energy covers a wide range of sources. Biomass gasification is a promising thermal process in which biomass can be converted into gas. This gas can then be used to produce valuable chemicals through the Fischer-Tropsch process [4]. Fischer-Tropsch synthesis (FTS) has attracted the interest of researchers as a promising route for the production of ultraclean transportation fuel [5,6]. Various metals such as Fe, Co, Ni, and Ru can be employed in this reaction as the active phase [7,8]. Iron catalyst has been regarded as a catalyst with high olefin selectivity and low cost with superior resistance against poisons in the synthesis gas [9]. The high activity of the water-gas shift of iron catalyst encourages its application in cases where the syngas is produced from coal or biomass [10]. In addition to proper function (activity and selectivity), industrial catalysts should exhibit strong resistance against deactivation. In this regard, studies on the deactivation of iron catalysts are necessary to achieve catalysts with a longer lifetime [11]. In the early 1920s, various deactivation mechanisms were studied in FTS; however, some controversies remained concerning the major reasons for catalyst deactivation [12]. Mimura *et al.* studied the effect of the support performance on the iron

*Corresponding author. E-mail: zohdi@eng.usb.ac.ir

oxide catalysts, the effect of the co-precipitation method on alumina oxide catalyst preparation, and the elimination and deactivation of the catalyst by CO_2 [13]. Understanding the selectivity, activity, and deactivation of the FTS catalyst is of significant industrial and scientific importance. Jiang *et al.* assessed the effect of supports and promoters in the FTS to achieve better reaction performance [14]. Rytter *et al.* also investigated the selectivity and activity of Co-based catalysts with Ni or Ru promoters on alumina, silica, and titanium support in the FTS [15].

Artificial neural network (ANN) has found extensive applications in the field of catalysis. ANN can be employed in studying the deactivation of catalysts, including methanol transformation into hydrocarbons [16]. Razmjooie *et al.* examined the impact of pressure, temperature, and feed ratio in the FTS by the design of experiment (DoE) and neural network in a fixed-bed reactor with mathematical models and experimental data [17]. Ghofran Pakdel *et al.* used the ANN method to study the effect of Ni loading on the deactivation model of Ni/Al_2O_3 catalyst in the FTS [18]. The simulated data were modeled by RSM and ANN, and results were compared with the random experimental data and DOE findings [19]. Ghofran Pakdel *et al*. employed an ANN strategy for model determination to describe the deactivation behavior of $Fe/\gamma\text{-}Al_2O_3$ catalyst [20]. By simulating the data beyond the experimental range, ANN can accelerate the determination of the deactivation model. Moreover, thanks to predicting the catalyst behavior beyond the empirical domain, this network is a proper technique to predict the behavior of expensive catalysts in the long run. In this regard, the present study uses a combined approach (ANN/GPLE) to assess the effect of Mn, Cr, and Zr promoters and their different loadings on the deactivation model and stability of the iron-based catalyst, using the data reported in literature [21].

ARTIFICIAL NEURAL NETWORK

Studies on brain structure have recently gained considerable popularity. This interest has resulted in the development of artificial neural networks (ANN) for solving complex problems. ANN can be used for the prediction and optimization of each process, especially multi-variable functions and nonlinear systems. The application of ANN is more common than the other modeling approaches; this network employs data optimization to find the best outputs [22].

ANN belongs to a class of mathematical models in which the architecture relies on the concept of neuron. In an ANN, inputs can be generally linked to the outputs by a transformation function through converting them into neurons with specific weights. Each neuron acts as a small computational engine which receives and processes the input and transforms it into the output [23]. Evaluation of the ANN implies the determination of its ability to present an acceptable solution to new inputs (not included in the training process). The performance of the ANN simulation can be evaluated by regression analysis of the empirical data and the network outputs. The lower the mean square error, the better the training of the input in the training section and the more precise the solutions. ANN can be explored to determine the activity of the catalyst in long run and select the deactivation model. The low prediction error of ANN for all the data confirms its reliability for estimating the activity of catalysts during an extended time of the stream.

EXPERIMENTAL

Catalyst Preparation

The catalysts were prepared using the precipitation technique according to (100-x)Fe/xMe/5Cu/17Si formula (Me: Cr, Mn, Zr, $x < 20$). In summary, a solution containing $Si(OC_2H_5)_4$, $Fe(NO_3)_3$ and $CuN_2O_6{:}2H_2O$ was precipitated by a third metal $Mn(NO_3)_2$, ($Cr(NO_3)_3$ or $ZrO(NO_3)_2$) for Fe/xMe/5Cu/17Si(100-x) using NH_4OH at 83 °C until reaching the pH of 8-9. The precipitates were then aged and cooled down for 17 h, followed by washing with deionized water and drying at 110 ℃ for 18-24 h. The products were finally calcinated at 300 ℃ for five h under an air atmosphere. More details on the synthesis procedure can be found elsewhere [21].

Reactor Test

To assess the intrinsic effects of deactivation on the parameters of GPLE model, the operating conditions were chosen according to the previous works [24,25] to minimize the effects of heat and mass transfer [21]. The reaction was conducted in a quartz micro-reactor (internal diameter of 8 mm). The sample (35-100 mg) was reduced at 280 ℃ under

hydrogen flow with a rate of 30 cc min^{-1} for 2 h. Before the reaction, He gas (30 cc min^{-1}) was employed for 15 min to clean the catalyst at the constant pressure and temperature (1.8 atm and 280 ℃, respectively). Catalyst activity was examined in the Fischer-Tropsch reaction at 280 ℃ and 1.8 atm with the feed ratio of 2:1 (H_2/CO). The products were analyzed by gas chromatography (Varian 3700) equipped with the FID and TCD detectors to analyze hydrocarbons and CO and CO_2, respectively. More details can be found elsewhere [21].

RESULTS AND DISCUSSIONS

ANN Performance for 90Fe10Cr Catalyst

The training stop process was investigated to reach the minimum error gradient for the 90Fe10Cr catalyst. The ANN results indicated 1.7727×10^{-7} minimum gradient error in the 24^{th} training period, which shows the network convergence. The training factor (μ) was 1×10^{-9} at the end of the 24^{th} training period. The best performance of the validation data was obtained in the 18^{th} period with a mean square error of 7.58×10^{-6}.

ANN Performance for 95Fe5Cr Catalyst

The training stop process was investigated based on reaching the minimum error gradient for the 95Fe5Cr catalyst. At the end of the 26^{th} training period, the minimum gradient error and μ were 3328×10^{-6} and 1×10^{-8}, respectively, indicating the network convergence. The best performance of the validation data was obtained in the 20^{th} period with a mean square error of 1.0868×10^{-5}.

ANN Performance for 90Fe10Zr Catalyst

The training stop process in the ANN was utilized based on reaching a minimum gradient error in the 35^{th} training period for a 10% Zr promoter. The results showed that at the end of the 35^{th} period, the gradient error was 4.0963×10^{-6} while μ was 1×10^{-10}. Constant network error after the 35^{th} period indicates its convergence. The best performance of the validation data was calculated in the 29^{th} period as 99.9234×10^{-6}.

ANN Performance for 95Fe5Zr Catalyst

The training stop process to reach minimum gradient error in the case of 95Fe5Zr showed the gradient error of 1.6663×10^{-5} in the 15^{th} period, reflecting the network convergence. At the end of the 15^{th} period, μ was 1×10^{-9}. The best performance of the validation data was obtained in the 9^{th} period as 1.1164×10^{-5}.

ANN Performance for 90Fe10Mn Catalyst

Gradient variation, mean square error, and regression analysis of the data for 90Fe10Mn catalyst indicated proper accordance of the regression curves for training, test, and validation data as well as all the empirical ones with the network outputs. In the training stop process, the minimum gradient error was 1.0946×10^{-5} attained in the 55^{th} period, indicating the network convergence. At the end of the 55^{th} period, μ was 1×10^{-8}. The best performance of the validation data was calculated in the 49^{th} period, with a mean square error of 8.1887×10^{-6}.

ANN Performance for 95Fe5Mn Catalyst

The training stop process was investigated for the 95Fe5Mn catalysts to reach the minimum gradient error. The results indicated that after the 17^{th} period, the gradient error got a constant value of 8.9035×10^{-6}, reflecting the network convergence. Moreover, μ was 1×10^{-7} at the end of the 17^{th} period. The best performance of the validation data (1.4086×10^{-5}) was obtained in the 11^{th} period.

Catalyst Deactivation Models

Modeling is a combination of mathematical, physical, and chemical concepts to describe a phenomenon or process *via* simulating a system. Determination of the optimal parameters of a process is one of the major advantages of the simulation. The deactivation model is based on the mathematical description of a catalyst to facilitate the analysis of its stability and rate variations. The mathematical models of deactivation are a precise method to predict the activity of the catalysts to design and simulate the reactor performance. The issues regarding the deactivation of the catalysts play a decisive role in the process design. The deactivation phenomenon is inevitable, as its examination can result in finding proper kinetics to decline the adverse impacts.

Equation (1) can be used to calculate the deactivation rate of catalyst (r_d):

$$\text{Deactivation rate} = \frac{\text{Rate of reaction at any time}}{\text{Initial reaction rate}} \quad (1)$$

$$-r_d = \frac{da}{dt} \quad (2)$$

The deactivation rate depends on the reaction temperature, reaction rate constant (k_d), and activation energy. It also depends on the (a-a*) parameter in which "a" shows the activity, while "a*" denotes the activity for infinite reaction duration. P_d also represents the partial pressure of deactivation compounds.

$$-r_d = k_d f(a, p_d) \quad (3)$$

GPLE model provides a proper form for the deactivation phenomenon. It tends to a limit value for long durations:

$$-r_d = -\frac{da}{dt} = k_d p_d^n (a - a^*)^\beta \quad (4)$$

As the dependence of the deactivation rate to the partial pressures of CO and H_2 was lower than its dependence on the activity and temperature, $k_d p_d^n$ can be substituted by $k_d^{"}$. β shows the deactivation order which can be used for fitting the data. For β = 1, GPLE is a first-order equation.

$$-r_d = -\frac{da}{dt} = k_d^{"}(a - a^*)^\beta \quad (5)$$

In Eq. (5), β shows the deactivation order; while a^* and $k_d^{"}$ represent the activity in long durations and deactivation constant, respectively.

$$-\frac{da}{(a-a^*)^\beta} = k_d^{"} dt \quad (6)$$

$$-\frac{1}{(1-\beta)}(a-a^*)^{1-\beta}\Big|_1^a = k_d^{"} t \rightarrow (a-a^*)^{1-\beta} - (1-a^*)^{1-\beta} = (\beta-1)k_d^{"} t \quad (7)$$

$$(a-a^*)^{1-\beta} = (1-a^*)^{1-\beta} + (\beta-1)k^{"}{}_d t \quad (8)$$

$$\beta \neq 1 \rightarrow a = a^* + [(1-a^*)^{1-\beta} + k^{"}(\beta-1)t]^{\frac{1}{1-\beta}} \quad (9)$$

$$\beta = 1 \rightarrow a = (1-a^*)\exp(-k_d^{"} t) + a^* \quad (10)$$

Deactivation Behavior of the Catalysts

Figure 1 shows the activities of the iron catalyst containing 5% promoters (Cr, Zr, and Mn). All of the catalysts had rapid and slow deactivation steps during the time of stream. Cr- and Zr-promoted catalysts rapidly deactivated in the first stage. During the first 50 min, 40% activity drop was observed for the Zr- and Cr-promoted catalysts. For Mn, the catalytic behavior declined with a milder slope over time. After 200 min, the activity trended to a constant value.

Figure 2 shows the deactivation behavior of the iron catalyst with a 10% promoter (Cr, Zr, and Mn). The number of stages of the activity drop and the slops of graphs are the same as the case for 5% promoter loadings. Sharper activity drops were observed during the fists 200 min. However, for the Cr- and Zr-promoted catalysts, 40% activity drop occurred during the first 25 min. As can be observed, the iron catalyst with the Mn promoter showed delayed deactivation compared to the other two promoters. This hypothesis can be further investigated by simulating the catalyst deactivation. A comparison between Figs. 1 and 2 shows the influence of the type and loading percentage of promoters on the activity drop during the reaction. Regarding the limited time of

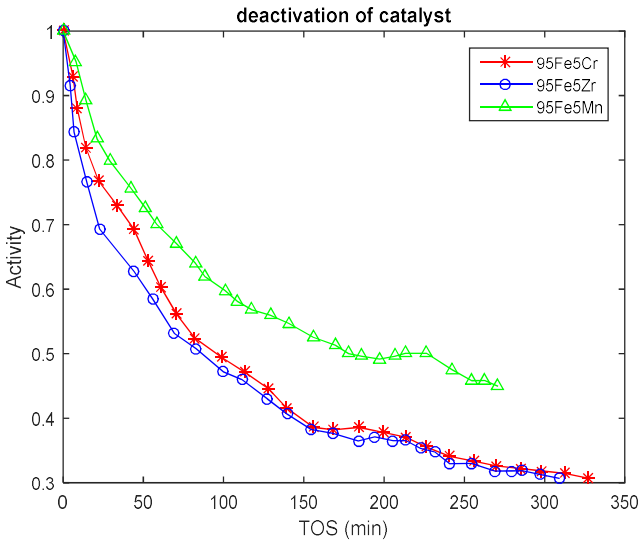

Fig. 1. Deactivation rate of the iron catalyst containing 5% Cr, Zr, and Mn [21].

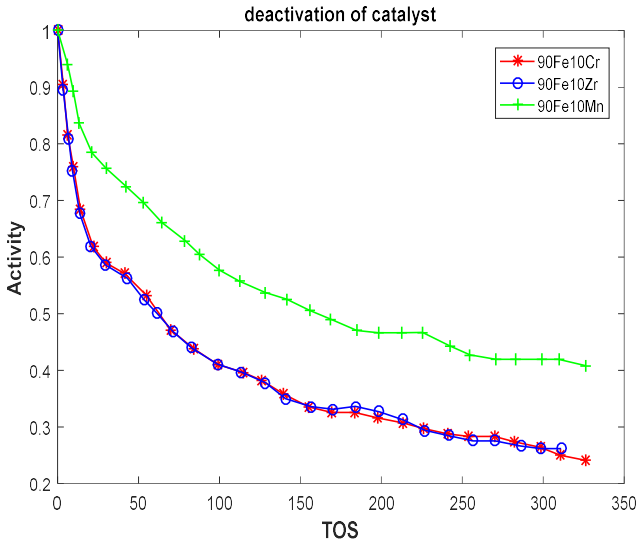

Fig. 2. Deactivation rate of the iron catalyst containing 10% Cr, Zr, and Mn [21].

experimental studies, the long-term catalyst activity was assessed using ANN.

In the Fe-based catalysts, the Fe_3O_4 phase may convert to iron carbides. Therefore, catalyst conversion rises during the reorganization of Fe-based catalysts, due to the activity of these phases in the FTS [26]. The formation of Fe_3O_4 by the oxidation of these carbides declines the activity of the catalyst during the on-stream procedure [27].

In this study, the onset of the deactivation study involved the pseudo steady-state condition (maximum point), where conversion did not rise during the on-stream time. Moreover, the ANN results demonstrated a decline in the activity for a long-time on-stream process, confirming the deactivation phenomenon. Depending on the operating conditions and catalyst composition, the on-stream time for approaching the steady-state conditions varied for different catalytic systems. Eliason *et al.* examined the deactivation kinetics of the promoted and un-promoted iron catalysts for a short-time stream (9 h) in the FTS [24]. Monzón *et al.* studied the relationship between the kinetic parameters of different catalyst deactivation models during 200 min of TOS [28].

Determination of the Proper Deactivation Models

To determine the appropriate deactivation model, the values obtained from the models were compared with the ANN results (Table 1), and the best model was determined for each promoter.

Table 1. a^* Parameter Obtained by the Hybrid ANN/ GPLE Technique

Catalyst	GPLE1 a^*	GPLE2 a^*	ANN a^*
90Fe10Cr	0.3	0.216	0.23
90Fe10Zr	0.315	0.228	0.26
90Fe10Mn	0.427	0.3	0.34
95Fe5Cr	0.322	0.168	0.31
95Fe5Zr	0.337	0.226	0.32
95Fe5Mn	0.457	0.3	0.42

According to Table 1, for the case of 90Fe10Cr, a^* value was equal to 0.3 in the first-order GPLE model, while for the second-order GPLE model, the amount of this parameter was 0.216. ANN predicted 0.23 for this parameter. According to ANN results, the second-order GPLE model was more appropriate as its a^* was closer to the actual value.

In the case of 90Fe10Zr, a^* value was 0.315 and 0.228 using the first and second-order GPLE models, respectively. The prediction of ANN was 0.26. According to ANN results, the second-order GPLE model was more appropriate as its a^* was closer to the actual value. The same results hold for the case of 90Fe10Mn. Therefore, the second-order GPLE model is more significant for the iron catalysts, including 10% promoters (Cr, Zr, and Mn).

According to Table 1, for the case of 95Fe5Cr, a^* value was 0.322 and 0.168 by the first and second-order GPLE models, respectively. The prediction of ANN was 0.31. Therefore, the first-order GPLE model was more appropriate as its a^* was closer to the actual value.

Considering 95Fe5Zr, a^* value was 0.337 and 0.226 by the first and second-order GPLE models, respectively. The prediction of ANN was 0.32. Therefore, the first-order GPLE model was more appropriate as its a^* was closer to the actual value. These results hold for the 95Fe5Mn catalyst as well. Thus, according to ANN results, the first-order GPLE model is more suitable for the catalysts containing 5% promoters (Cr, Zr, and Mn).

Based on the obtained results, the second-order GPLE model was better for the catalysts containing 10% promoters, while the first-order one was more appropriate for the catalysts containing 5% promoters. Coking [29] and sintering [30] deactivation are usually well fitted by the first-order and second-order GPLE, respectively. Consequently, the promoter loadings of 5% and 10% indicated coking and sintering mechanisms, respectively.

Model Validation

To validate the determined models, the predicted values were compared with the new data. Tables 2-4 present the validation results.

As seen, the data predicted by the second-order deactivation model well matched with the data related to the catalysts containing 10% promoter. Whereas, the first-order model offered proper fitting for the catalyst with 5% promoter.

Effect of the Promoter on the Parameters of the Deactivation Models

Table 5 lists the parameters of deactivation models for iron catalysts containing 10 and 5% promoters (Cr, Zr, and Mn). Regression analysis was based on the Levenberg-Marquardt algorithm which can be employed for nonlinear problems. K_d is the deactivation constant. The higher the deactivation constant, the sooner the catalyst deactivation.

Based on Table 5, the deactivation constant of the samples with 5% and 10 % promoters were compared considering the first-order and second-order GPLE models, respectively.

For various promoter loadings, the Zr promoter increased the deactivation rate of iron catalysts. A comparison of the steady-state activity of the catalysts with varying promoter content indicated that the iron catalysts containing Mn promoter had higher stability. For 5% loading of Mn, a^* value was 42% based on ANN prediction. Its 10% loading resulted in 0.34 activity; therefore, the steady-state activity of 5% Mn was higher.

CONCLUSIONS

Catalyst deactivation plays a destructive role in many industrial applications. This phenomenon and its environmental consequences are among the serious challenges of industry; since halting the process and

Table 2. Validation of the Second-order GPLE Model for 90Fe10Cr and First-order GPLE Model Validation for 95Fe5Cr

	Activity (90Fe10Cr)		Activity (95Fe5Cr)	
Run	Experimental	Model	Experimental	Model
1	1	1	1	1
2	0.866	0.869	0.909	0.932
3	0.746	0.775	0.783	0.844
4	0.632	0.667	0.668	0.665
5	0.542	0.492	0.605	0.608
6	0.453	0.416	0.526	0.536
7	0.403	0.374	0.474	0.459
8	0.363	0.347	0.423	0.419
9	0.328	0.328	0.379	0.393
10	0.323	0.314	0.379	0.366
11	0.298	0.302	0.352	0.350
12	0.284	0.293	0.336	0.340
13	0.279	0.286	0.324	0.335
14	0.254	0.28	0.316	0.330

Table 3. Validation of the Second-order GPLE Model for 90Fe10Zr and First-order GPLE Model Validation for 95Fe5Zr

	Activity (90Fe10Zr)		Activity (95Fe5Zr)	
Run	Experimental	Model	Experimental	Model
1	1	1	1	1
2	0.833	0.863	0.871	0.917
3	0.731	0.767	0.742	0.811
4	0.626	0.686	0.658	0.69
5	0.572	0.564	0.569	0.563
6	0.521	0.475	0.505	0.476
7	0.439	0.416	0.445	0.418
8	0.397	0.375	0.406	0.388
9	0.358	0.351	0.366	0.368
10	0.327	0.334	0.366	0.356
11	0.327	0.319	0.346	0.348
12	0.307	0.309	0.336	0.344
13	0.272	0.300	0.317	0.341
14	0.264	0.293	0.316	0.339

Table 4. Validation of the Second-order GPLE Model for 90Fe10Mn and First-order GPLE Model Validation for 95Fe5Mn

	Activity (90Fe10Mn)		Activity (95Fe5Mn)	
Run	Experimental	Model	Experimental	Model
1	1	1	1	1
2	0.904	0.933	0.946	0.939
3	0.778	0.832	0.838	0.875
4	0.707	0.696	0.788	0.814
5	0.619	0.607	0.707	0.704
6	0.556	0.555	0.617	0.619
7	0.523	0.519	0.576	0.569
8	0.498	0.494	0.536	0.531
9	0.464	0.47	0.531	0.512
10	0.46	0.453	0.5	0.493
11	0.43	0.44	0.491	0.482
12	0.41	0.429	0.455	0.472
13	0.414	0.419	0.446	0.467
14	0.41	0.414	0.445	0.464

Table 5. Effects of Promoters on the Parameters of Deactivation Models

Catalyst	Order	a^*	k_d	R^2	R^2_{adj}
90Fe10Cr	2	0.216	0.0457	0.985	0.984
90Fe10Zr	2	0.228	0.05	0.981	0.98
90Fe10Mn	2	0.3	0.023	0.993	0.992
95Fe5Cr	1	0.322	0.016	0.991	0.991
95Fe5Zr	1	0.337	0.018	0.973	0.972
95Fe5Mn	1	0.457	0.014	0.995	0.994

replacement or reconstruction of the catalyst in the reactor can be a costly stage. ANN can adequately determine the deactivation model and estimate the activity of the catalyst in the long run. This study assessed the effects of promoter type and loading percentage on the activity and stability of Fe-based catalyst that was synthesized by the precipitation technique. The results obtained by the hybrid ANN/GPLE technique indicated the influence of the promoter loading on the deactivation model of the iron catalyst. For the iron catalyst containing 10% promoter, the second-order GPLE model could reasonably predict the results, while for the iron catalyst including 5% promoter, the first-order GPLE model performed better in fitting with empirical data. For various promoters, Zr increased the deactivation constant, while Mn promoted the long-term performance of the catalyst. The steady-state activity of the catalysts containing 5 and 10% Mn was 0.42 and 0.32, respectively. Therefore, the iron catalyst containing a 5% promoter had higher stability. Compared to Zr and Cr, Mn promoter could play a decisive role in prolonging the catalyst lifetime and enhancing its activity. Validation analysis demonstrated that the ANN/GPLE hybrid technique could adequately predict the steady-state activity of the catalyst during on-stream time.

ACKNOWLEDGMENTS

The authors appreciate the financial and instrumental support from the University of Sistan and Baluchestan.

REFERENCES

[1] Del Monte, D. M.; Vizcaíno, A.; Dufour, J.; Martos, C., Effect of K, Co and Mo addition in Fe-based catalysts for aviation biofuels production by Fischer-Tropsch synthesis, *Fuel Process. Technol.* **2019**, *194*, 106102, DOI: 10.1016/j.fuproc.2019.05.025.

[2] Benedetti, V.; Ail, S. S.; Patuzzi, F.; Cristofori, D.; Rauch, R.; Baratieri, M., Investigating the feasibility of valorizing residual char from biomass gasification as catalyst support in Fischer-Tropsch synthesis, *Renewable Energy,* **2020**, *147*, 884-894, DOI: 10.1016/j.renene.2019.09.050.

[3] Atashi, H.; Zohdi-Fasaei, H.; Farshchi Tabrizi, F.; Mirzaei, A. A., Two-level Full Factorial Design for Selectivity Modeling and Studying Simultaneous Effects of Temperature and Ethanol Concentration in Methanol Dehydration Reaction, *Phys. Chem. Res.* **2017**, *5* (1), 41-56, DOI: 10.22036/pcr.2017.33491.

[4] Ren, J.; Cao, J. -P.; Zhao, X. -Y.; Yang, F. -L.; Wei, X. -Y., Recent advances in syngas production from biomass catalytic gasification: A critical review on reactors, catalysts, catalytic mechanisms and mathematical models, *Renewable Sustainable Energy Rev.* **2019**, *116*, 109426, DOI: 10.1016/ j.rser.2019.109426.

[5] Xu, R.; Hou, C.; Xia, G.; Sun, X.; Li, M.; Nie, H.; Li, D., Effects of Ag promotion for Co/Al_2O_3 catalyst in Fischer-Tropsch synthesis, *Catal. Today.* **2020**, *342*, 111-114, DOI: 10.1016/j.cattod.2019.04.004.

[6] Iliuta, I.; Larachi, F., Fischer-Tropsch synthesis in vertical, inclined and oscillating trickle-bed reactors for offshore floating applications, *Chem. Eng. Sci.* **2018**, *177*, 509-522, DOI: 10.1016/j.ces.2017.12.012.

[7] Ghofran Pakdel, M.; Atashi, H.; Zohdi-Fasaei, H.; Mirzaei, A. A., Effect of temperature on deactivation models of alumina supported iron catalyst during Fischer-Tropsch synthesis, *Pet. Sci. Technol.,* **2019**, *37* (5), 500-505, DOI: 10.1080/10916466.2018.1501389.

[8] MohammadRezapour, M.; Mirzaei, A. A.; Zohdi-Fasaei, H., Optimizing the preparation conditions of silica supported Fe-Co-Ce ternary catalyst for the fixed-bed Fischer-Tropsch synthesis: Taguchi experimental design approach, *Phys. Chem. Res.* **2018**, *6* (2), 387-397, DOI: 10.22036/pcr.2018.118835.1467.

[9] Zhang, S.; Li, D.;Liu, Y.; Zhang, Y.; Wu, Q., Zirconium doped precipitated Fe-based catalyst for Fischer-Tropsch synthesis to light olefins at industrially relevant conditions, *Catal. Lett.* **2019**, *149* (6), 1486-1495, DOI: 10.1007/s10562-019-02775-x.

[10] Yang, Y.; Xiang, H. -W.; Xu, Y. -Y.; Bai, L.; Li, Y. -W., Effect of potassium promoter on precipitated iron-manganese catalyst for Fischer-Tropsch synthesis, *Appl. Catal., A.* **2004**, *266* (2), 181-194, DOI: 10.1016/j.apcata.2004.02.018.

[11] Zhang, Y.; Cao, C.; Zhang, C.; Zhang, Z.; Liu, X.; Yang, Z.; Zhu, M.; Meng, B.; Xu, J.; Han, Y. -F., The study of structure-performance relationship of iron catalyst during a full life cycle for CO_2 hydrogenation,

J. Catal. **2019**, *378*, 51-62, DOI: 10.1016/j.jcat.2019.08.001.

[12] Peña, D.; Cognigni, A.; Neumayer, T.; Van Beek, W.; Jones, D. S.; Quijada, M.; Rønning, M., Identification of carbon species on iron-based catalysts during Fischer-Tropsch synthesis, *Appl. Catal., A.* **2018**, *554*, 10-23, DOI: 10.1016/j.apcata.2018.01.019.

[13] Mimura, N.; Saito, M., Dehydrogenation of ethylbenzene to styrene over Fe_2O_3/Al_2O_3 catalysts in the presence of carbon dioxide, *Catal. Lett.* **1999**, *58* (1), 59-62, DOI: 10.1023/A:1019049127309.

[14] Jiang, F.; Zhang, M.; Liu, B.; Xu, Y.; Liu, X., Insights into the influence of support and potassium or sulfur promoter on iron-based Fischer-Tropsch synthesis: understanding the control of catalytic activity, selectivity to lower olefins, and catalyst deactivation, *Catal. Sci. Technol.* **2017**, *7* (5), 1245-1265, DOI: 10.1039/C7CY00048K.

[15] Rytter, E.; Skagseth, T. H.; Eri, S.; Sjåstad, A. O., Cobalt Fischer-Tropsch catalysts using nickel promoter as a rhenium substitute to suppress deactivation, *Ind. Eng. Chem. Res.* **2010**, *49* (9), 4140-4148, DOI: 10.1021/ie100308f.

[16] Kito, S.; Satsuma, A.; Ishikura, T.; Niwa, M.; Murakami, Y.; Hattori, T., Application of neural network to estimation of catalyst deactivation in methanol conversion, *Catal. Today.* **2004**, *97* (1), 41-47, DOI: 10.1016/j.cattod.2004.04.052.

[17] Razmjooie, A.; Atashi, H.; Shahraki, F., Analysis of the effective operating factors of Fischer-Tropsch synthesis; Investigation of modeling and experimental data, *J. Nat. Gas Sci. Eng.* **2017**, *40*, 72-78, DOI: 10.1016/j.jngse.2017.02.004.

[18] Ghofran Pakdel, M.; Zohdi-Fasaei, H.; Mirzaei, A. A.; Atashi, H., Neural Computing Strategy for Predicting Deactivation of Fischer-Tropsch Synthesis With Different Nickel Loadings, *Catal. Lett.* **2019**, *149* (9), 2444-2452, DOI: 10.1007/s10562-019-02860-1.

[19] Shiva, M.; Atashi, H.; Farshchi Tabrizi, F.; Mirzaei, A. A.; Zare, A., The application of hybrid DOE/ANN methodology in lumped kinetic modeling of Fischer-Tropsch reaction, *Fuel Process. Technol.* **2013**, *106*, 631-640, DOI: 10.1016/j.fuproc.2012.09.056.

[20] Ghofran Pakdel, M.; Atashi, H.; Mirzaei, A. A.; Zohdi-Fasaei, H., Deactivation Model for an Industrial γ-Alumina Supported Iron Catalyst in the Fischer Tropsch Synthesis, *Chem. Select.* **2019**, *4* (7), 2064-2069, DOI: 10.1002/slct.201802140.

[21] Lohitharn, N.; Goodwin Jr, J. G., Impact of Cr, Mn and Zr addition on Fe Fischer-Tropsch synthesis catalysis: Investigation at the active site level using SSITKA, *J. Catal.* **2008**, *257* (1), 142-151, DOI: 10.1016/j.jcat.2008.04.015.

[22] Adib, H.; Haghbakhsh, R.; Saidi, M.; Takassi, M. A.; Sharifi, F.; Koolivand, M.; Rahimpour, M. R.; Keshtkari, S., Modeling and optimization of Fischer-Tropsch synthesis in the presence of $Co(III)/Al_2O_3$ catalyst using artificial neural networks and genetic algorithm, *J. Nat. Gas Sci. Eng.* **2013**, *10*, 14-24, DOI: 10.1016/j.jngse.2012.09.001.

[23] Khorashadizadeh, M.; Atashi, H.; Mirzaei, A. A., Process conditions effects on Fischer-Tropsch product selectivity: Modeling and optimization through a time and cost-efficient scenario using a limited data size, *J. Taiwan Inst. Chem. Eng.* **2017**, *80*, 709-719, DOI: 10.1016/j.jtice.2017.09.006.

[24] Eliason, S.; Bartholomew, C., Reaction and deactivation kinetics for Fischer-Tropsch synthesis on unpromoted and potassium-promoted iron catalysts, *Appl. Catal., A.* **1999**, *186* (1-2), 229-243, DOI: 10.1016/S0926-860X(99)00146-5.

[25] Lohitharn, N.; Goodwin Jr, J. G.; Lotero, E., Fe-based Fischer-Tropsch synthesis catalysts containing carbide-forming transition metal promoters, *J. Catal.* **2008**, *255* (1), 104-113, DOI: 10.1016/j.jcat.2008.01.026.

[26] Riedel, T.; Schulz, H.;Schaub, G.; Jun, K. -W.; Hwang, J. -S.; Lee, K. -W., Fischer-Tropsch on iron with H_2/CO and H_2/CO_2 as synthesis gases: the episodes of formation of the Fischer-Tropsch regime and construction of the catalyst, *Top. Catal.* **2003**, *26* (1), 41-54, DOI: 10.1023/B:TOCA.0000012986.46680.28.

[27] Ning, W.; Koizumi, N.; Chang, H.; Mochizuki, T.; Itoh, T.; Yamada, M., Phase transformation of unpromoted and promoted Fe catalysts and the formation of carbonaceous compounds during Fischer-Tropsch synthesis reaction, *Appl. Catal., A.* **2006**, *312*, 35-44, DOI: 10.1016/j.apcata.2006.06.025.

[28] Monzón, A.; Romeo, E.; Borgna, A., Relationship

between the kinetic parameters of different catalyst deactivation models*, Chem. Eng. J.* **2003**, *94* (1), 19-28, DOI: 10.1016/S1385-8947(03)00002-0.

[29] Bartholomew, C. H., Mechanisms of catalyst deactivation*, Appl. Catal., A.* **2001**, *212* (1-2), 17-60, DOI: 10.1016/S0926-860X(00)00843-7.

[30] Argyle, M.; Frost, T.; Bartholomew, C., Cobalt Fischer-Tropsch catalyst deactivation modeled using generalized power law expressions*, Top. Catal.* **2014**, *57* (6), 415-429, DOI: 10.1007/s11244-013-0197-9.